Materials Research. 2016; 19(3): 548-554
DOI:http://dx.doi.org/10.1590/1980-5373-MR-2016-0017

A study on the microstructural parameters of $Zn_{(1-x)}La_xZr_xO$ nanopowders by X-ray line broadening analysis

***Hossein Mahmoudi Chenari*[a]*, *Hadi Fallah Moafi*[b], *Omid Rezaee*[a]**

[a]*Department of Physics, Faculty of Science, University of Guilan, Namjoo Ave, Po Box 41335-1914, Rasht, Iran*
[b]*Department of Chemistry, Faculty of Science, University of Guilan, Namjoo Ave, Po Box 41335-1914, Rasht, Iran*

Received: January 25, 2016; Accepted: March 7, 2016

In the present study, the pure and La-Zr co-doped ZnO nanoparticles were prepared by sol–gel technique using zinc acetate dehydrate ($Zn(Ac)_2 \cdot 2H_2O$), lanthanum nitrate hexahydrate ($La(NO_3)3 \cdot 6H_2O$) and zirconium chloride ($ZrCl_4$) as precursor. The structure and morphology of the prepared nanoparticle samples were studied using X-ray diffraction and transmission electron microscopy measurements. X-ray diffraction results indicated that all the samples have crystalline wurtzite phase. TEM showed that powder was polycrystalline in nature with random distribution of the pure and La-Zr doped ZnO nanoparticles. We demonstrate strain-size evaluations for pure and doped ZnO nanoparticles from the x-ray line profile analysis. The microstructural effects of crystalline materials in terms of crystallite sizes and lattice strain on the peak broadening were investigated using Williamson-Hall (W-H) analysis and size- strain plot (SSP) method. The average crystallite size of $Zn_{(1-x)}La_xZr_xO$ nanoparticles estimated from the W–H analysis and SSP method varied as the doping concentration increased. The incorporation of Zr^{4+} ion in the place of Zn^{2+} caused an increase in the size of nanocrystals as compared to undoped ZnO. The average particle sizes of co-doped ZnO nanoparticles estimated from the USDM model is in good agreement with the TEM results.

Keywords: *ZnO; X-ray diffraction; TEM; Williamson-Hall analysis; SSP model*

1. Introduction

Nano-structured metal oxide semiconductors are gaining attention due to their wide band-gap and related properties. Among the semiconducting materials, zinc oxide (ZnO) is a promising candidate due to its excellent physical and chemical properties for a wide range of applications such as varistors, luminescence, electrostatic dissipative coatings, transparent UV protection films, chemical sensors, etc. [1-5]. ZnO nanoparticles in both powder and film form can be synthesized using various methods such as chemical vapor deposition, chemical spray pyrolysis , sol-gel technique , and hydrothermal treatment [6-10]. ZnO is doped with different types of metallic ions in order to enhance the optical and conducting properties [11]. In the recent times, transition metal-doped ZnO (e.g., La, Zr,…) has been broadly researched and concentrated on luminescence properties, magnetic, optical and photocatalytic activity, sensor and memory applications [12-20]. It is evident that the materials in a nanometer scale have a large surface area and surface energy of the system. Therefore, a simple relaxation (expansion or contraction) of the crystalline lattice may lead to stabilization of metastable nanostructure. The change in lattice parameter of metal-doped ZnO powders is dependent upon the ionic radius of doping ion, which can substitute the Zn ion in the lattice [21]. The ionic radius of the dopant ion is important factor, which can strongly influence the ability of the dopant to enter into oxides crystal lattice. If the ionic radius of the doping metal ions matches those of the lattice metal ion in oxides, the doping metal ion will substitute itself for the lattice in the doping reactive process (substitutional mode). Whereas, the ions with the radius which are much bigger or smaller than that of metal ion in oxides cause crystal lattice distortion [22,23]. In the doping reactive process it can either isomorphously substituted or interstitially introduced into the matrix of ZnO to produce oxygen vacancies which accelerate the nanocrystallite growth of wurtzite ZnO [24]. In addition, La–Zr co-doped ZnO did not give any peak corresponding to ZrO2 or La2O3, possibly demonstrating that La3+ and Zr4+ were dispersed uniformly onto ZnO nanoparticles as the form of small cluster La2O3 or ZrO2. This is due to the formation of nanosize particles in the range undetectable by XRD. X-ray profile analysis is a simple and powerful tool to estimate the crystallite size and lattice strain [25] . There are many analytical techniques to evaluate the microstructure properties of materials [26-29]. To our knowledge, from the point of view of the microstructural properties, comparing many reported nanostructures synthesised, little work has been carried out to evaluate the microstructure properties of La–Zr doped ZnO nanopowders. This study highlights the microstructure analysis of La–Zr doped ZnO nanoparticles. The present work highlights the structure and morphology of pure and co-doped ZnO nanoparticles by X-ray diffraction

*e-mail: mahmoudi_hossein@guilan.ac.ir, hmahmodiph@yahoo.com

analysis (XRD) and transmission electron microscopy (TEM). From the modified Williamson- Hall procedure and the size-strain plot (SSP) method, we give more information on strain-stress and the energy density of pure and doped ZnO nanoparticles. A comparative evaluation of the mean particle size of pure and doped ZnO nanoparticles obtained from direct TEM measurements and from powder X-ray diffraction (XRD) peak broadening is also investigated.

2. Experimental Details

La–Zr co-doped ZnO nanoparticles were synthesized by a simple sol-gel route which its details reported elsewhere [30]. We will discuss in the following the results of the structure analysis and the chemical composition measurements. The bulk sensitive X-ray diffraction (XRD) patterns were taken with Philips X'Pert diffractometer at room temperature using monochromatic Cu Kα (hν = 8042.55 eV) excitation. Measurements were taken under beam acceleration conditions of 40 kV/35 mA. The surface sensitive transmission electron spectroscopy (TEM) measurements were obtained on a Philips, CM10 instrument with an accelerating voltage of 100 kV.

3. Results and Discussion

3.1. Methods of X-ray profile analysis

X-ray diffraction line profile analysis is one of the earliest methods which is conventionally used to study the physical and microstructural parameters of polycrystalline materials. Many new methods have been proposed to extract microstructural information from the XRD line profile. Fig. 1(a, b, c, d) shows the x-ray diffractogram of the $Zn_{(1-x)}La_xZr_xO$ nanoparticles; x=0,0.02,0.04,0.06. A preferable growth along the {101}, {002}, {100}, {102}, {110} and {103} directions could be indexed as hexagonal wurtzite phase of ZnO as according to the JPCDS card number: 36-1451 [31]. The calculated lattice parameters of the La-Zr co-doped ZnO nanoparticles are a=b=3.2264 A^0, c=5.1739 A^0 are closely well agreement with the reported values (JCPDS Card No. 01-089-0510). In addition, La–Zr co-doped ZnO did not give any peak corresponding to ZrO2 or La2O3, possibly demonstrating that La^{3+} and Zr^{4+} were dispersed uniformly onto ZnO nanoparticles. As it's evident from the table 1, the crystallite size of ZnO nanoparticles increasees with increasing La-Zr ratio. The right graph in the Fig. 1 shows a negligible shift in (110) Brag reflection for the samples with a different amount of La-Zr compared to the ZnO nanoparticles. This shift could be attributed to the strain in the lattice of compounds. Also, it is expected the replacement of some Zn^{2+} ions with the Zr^{4+} in each compound due to their different ionic radius. In order to find the effect of strain on the peak broadening, we use a modified equation and adopted the following techniques of line profile analysis to obtain microstructural information from the symmetrically broadened diffraction profiles.

3.1.1. Williamson-Hall Technique

In almost all cases X-ray diffraction profiles are influenced not only by crystallite size but also possibly by lattice strain and lattice defects. Williamson and Hall proposed a method for deconvoluting size and strain broadening by looking at the peak width as a function of 2θ. However it makes some very large assumptions along the way [32-34]. According to the Williamson–Hall (W-H) method the individual contribution to the line broadening of a Bragg reflection can be expressed as [35]

$$\beta_{hkl} = \beta_D + \beta_\varepsilon \quad (1)$$

$$\beta_{hkl} Cos\theta = (k\lambda / D) + 4\varepsilon \sin\theta \quad (2)$$

Where β_{hkl} is the peak width at half-maximum intensity, β_D is due to the contribution of crystallite size, β_ε is the peak broadening due to the strain (ε) and D is the average crystallite size of a X-ray peak. In the Eq. 2 the strain was assumed to be uniform in all crystallographic direction implying a uniform deformation model ('UDM'). Fig. 2 shows the UDM analysis. The term (β_{hkl} Cosθ) is plotted versus (4Sinθ). The effective crystallite size can be estimated from the extrapolation on the plot and the slop of the fitted line represents the strain. Deviation from the straight line fit in Fig. 2 represents that an anisotropic approach such as

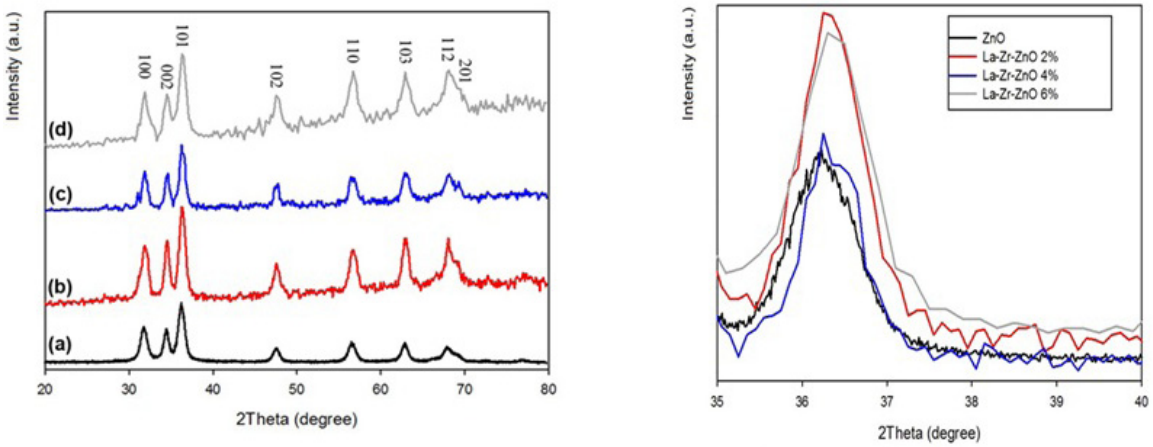

Fig.1. Powder X-raydiffraction data of (a) ZnO, (b) Zn0.98La0.02 Zr0.02O, (c) Zn0.96La 0.04Zr 0.04O, and (d) Zn0.94La 0.06 Zr 0.06O nanoparticles. The right graph shows doping-induced (002) peak shift with La–Zr elements in the ZnO matrix.

Table 1. Microstructural paprameters of $Zn_{(1-x)}La_xZr_xO$ nanoparticles.

Ba Concentration (x)	Williamson - Hall Method									Size – Strain Plot Method					TEM
	UDM		USDM			UDEDM									
	D (nm)	ε×10^{-3} (no unit)	D (nm)	σ (MPa)	ε×10^{-3} (no unit)	D (nm)	u (Kj m^{-3})	ε×10^{-3} (no unit)	σ (MPa)	D (nm)	ε×10^{-3} (no unit)	σ (MPa)	u (Kj m^{-3})	Std. Error	D (nm)
0	18.83	5.83	18.46	742.22	5.84	18.73	21.82	5.86	744.22	39.68	2.802	355.85	49.855	1.6032E-06	≈35[7]
0.02	22.48	6.23	22.31	801.56	6.31	22.55	25.19	6.29	798.83	47.17	1.529	194.18	14.845	1.7306E-06	-
0.04	33.83	5.26	25.93	582.47	4.59	29.11	15.06	4.87	618.49	53.57	3.654	484.06	92.249	3.2920E-06	-
0.06	59.09	10.24	52.77	1436.29	11.31	76.38	87.73	11.75	1492.25	67.57	1.838	233.43	21.453	7.1333E-07	50

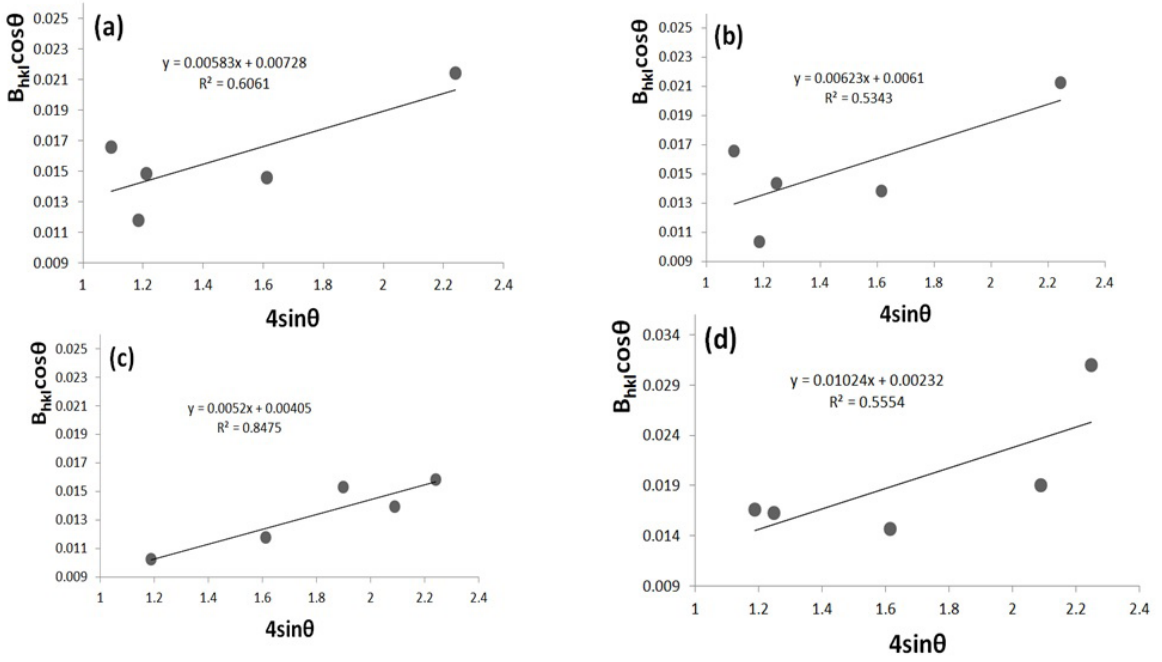

Fig. 2. W-H analysis of (a) ZnO, (b) Zn0.98La0.02 Zr0.02O, (c) Zn0.96La 0.04Zr 0.04O, and (d) Zn0.94La 0.06 Zr 0.06O nanoparticles assuming assuming UDM model.

uniform stress deformation model (USDM) and uniform deformation energy density model (UDEDM) should be adopted in the W-H approach. In the USDM, stress (σ) is related to the strain (ε) as $\sigma=Y_{hkl}\,\varepsilon$, where Y_{hkl} is young's modulus and given by

$$Y_{hkl}=\frac{[h2+\frac{(h+2k)2}{3}+\frac{(al)2}{3}]2}{s_{11}(h^2+\frac{(h+2k)^2}{3})+s_{33}(\frac{al}{c})^4+(4s_{13}+s_{44})(h^2\frac{(h+2k)^2}{3})(al/c)^2} \quad (3)$$

For the hexagonal crystals, Where s_{11}, s_{13}, s_{33}, s_{44} are the elastic compliances of ZnO with values of 7.858 x 10^{-12}, -2.206 x 10^{-12}, 6.940x10^{-12}, 23.57 x10^{-12} $m^2\,N^{-1}$, respectively [36]. For La–Zr co-doped ZnO, Young's modulus was calculated as ≈127 GPa. The modified form of W-H equation assuming USDM will be of the form

$$\beta_{hkl}Cos\theta = (k\lambda/D) + 4(\sigma\,Sin\theta)/Y_{hkl} \quad (4)$$

The USDM plots are shown in the Fig. 3 and the microstrucrural results are listed in Table 1. In the modified W–H equation based on a uniform deformation energy density model (UDEDM), the young modulus and strain are connected to the deformation energy density 'u' by $u=\varepsilon^2/2Y_{hkl}$ and the Eq. 4. can be modified according the energy and strain relation as

$$\beta_{hkl}Cos\theta = (k\lambda/D) + \left(4\,\sin\theta\left(2u/Y_{hkl}\right)^{1/2}\right) \quad (5)$$

From the plots of β_{hkl} Cosθ versus 4 sinθ$(2u/Y_{hkl})^{1/2}$, the anisotropic energy density (u) and the crystallite size can be estimated from the slope and the y-intercept of fitted line, respectively **(see** Fig. 4**)**. The USDM results are collected in table 1. As can be seen from the table 1, the crystallite sizes calculated from various models are approximately same, which indicate that the inclusion of strain in various W–H models has a very small effect on the average crystallite size of ZnO nanoparticles.

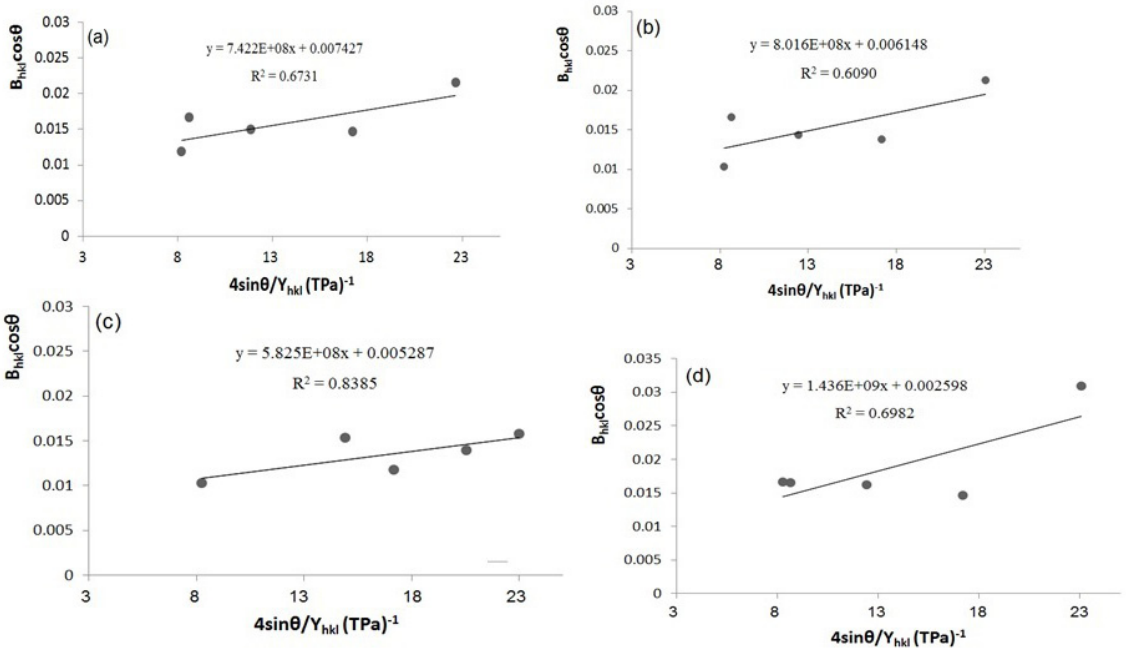

Fig. 3. The modified form of W-H analysis assuming USDM for (a) ZnO, (b) Zn0.98La0.02 Zr0.02O, (c) Zn0.96La 0.04Zr 0.04O, and (d) Zn0.94La 0.06 Zr 0.06O nanoparticles.

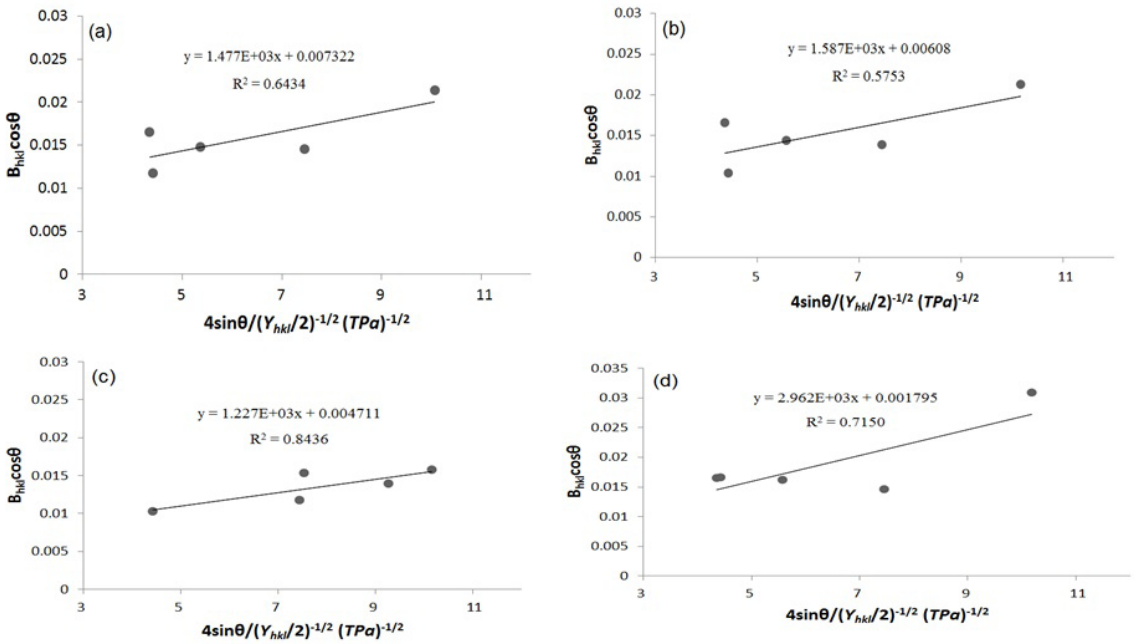

Fig. 4. The modified form of W-H analysis assuming UDEDM for (a) ZnO, (b) Zn0.98La0.02 Zr0.02O, (c) Zn0.96La 0.04Zr 0.04O, and (d) Zn0.94La 0.06 Zr 0.06O nanoparticles.

3.1.2. Size- Strain plot method

Size-strain plot method is another procedure to obtain the size-strain parameters. This method is constructed according to the following relation:

$$(d_{hkl}\beta_{hkl}\cos\theta)^2 = \frac{k}{D}(d^2{}_{hkl}\beta_{hkl}\cos\theta) + (\frac{\varepsilon}{2})^2 \quad (6)$$

Where d_{hkl} is the lattice distance between the <hkl> planes and k is a constant and depends on the shape of the particles (for spherical particles k= ¾ [37]. Plot of $(d^2_{hkl}\beta_{hkl}\cos\theta)$ versus $(d_{hkl}\beta_{hkl}\cos\theta)^2$ were constructed for the all Bragg reflection of La–Zr co-doped ZnO nanoparticles (see Fig. 5). In this method less importance is given to data from reflections at high angles and the crystallite size distribution is

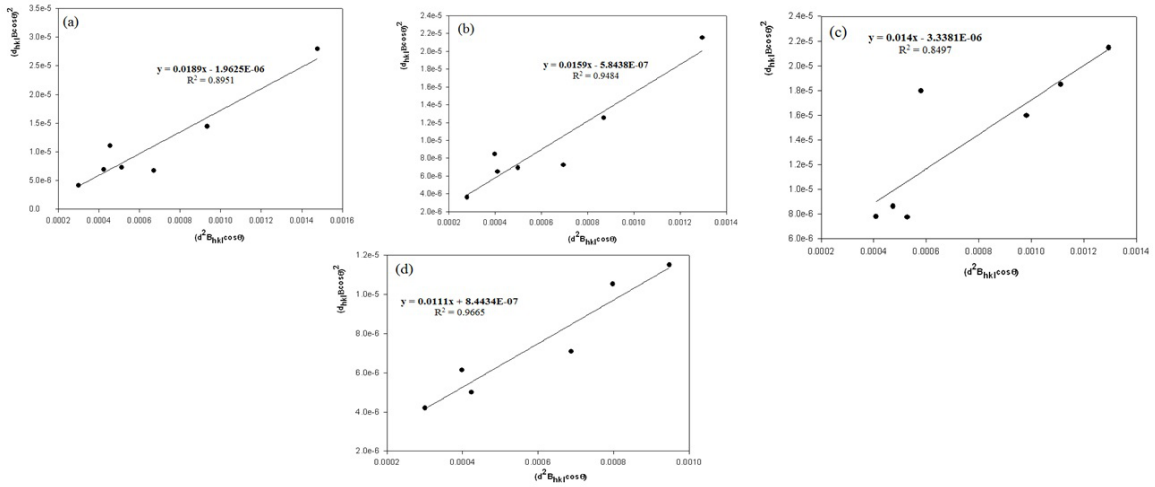

Fig. 5. The SSP plot of a) ZnO, (b) Zn0.98La0.02 Zr0.02O, (c) Zn0.96La 0.04Zr 0.04O, and (d) Zn0.94La 0.06 Zr 0.06O nanoparticles.

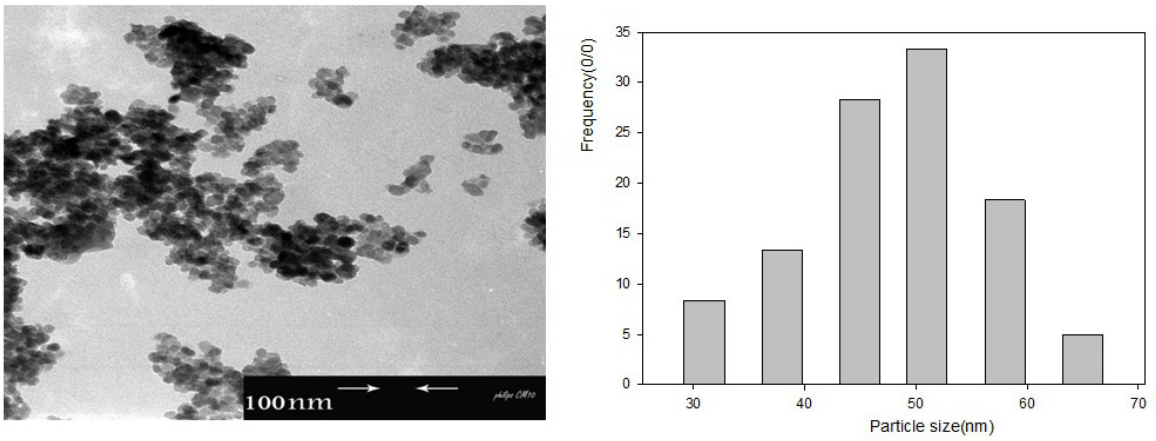

Fig. 6. TEM image and the particle size distribution of Zn0.94La0.06Zr0.06 nanoparticles.

described by a Lorentzian function and the strain by a Gaussian function [38]. The strain is given from the root of the y-intercept and slop gives the particle size. The results attained from the SSP models are summarized in table 1. It was observed from the table 1 that the crystallite size of the La–Zr co-doped ZnO nanoparticles increased with increase in the La–Zr concentration. The polycrystalline show a larger value of ε indicating more strain on the lattice. The larger strain induced by the internal stress could lead to peak broadening.

3.2. TEM Method

The size and shape of the La–Zr co-doped ZnO nanoparticles could be best examined by TEM measurements. TEM image for the pure ZnO nanoparticles was obtained according to the method described elsewhere [30] about 35 nm. Fig. 6 displays a TEM image and particle size distribution of the Zn0.94La0.06Zr0.06 nanoparticles. As it's clear from the particle size distribution, the width of the nanoparticles varies from 25 to 65nm with an average particle size of 50 nm. The average size obtained from the TEM analysis is in good agreement with the results of the USDM model.

4. Conclusions

The pure and La-Zr co-doped ZnO nanoparticles prepared by a simple sol-gel method were characterized by powder X-ray diffraction (XRD) and TEM measurement. XRD analysis shows that the prepared samples are in hexagonal wurtzite phase and free of any other Zr-La phase after doping. The size and strain contributions to line broadening were studied using the X-ray peak broadening analysis by the Williamson–Hall method and the size-strain plot (SSP) method. The crystallite sizes calculated from various models are approximately same, which indicate that the inclusion of strain has a very small effect on the average crystallite size of ZnO nanoparticles. The average particle size obtained from the TEM results is in good agreement with the results of the USDM model.

References:

1. Gao PX, Ding Y, Mai W, Hughes WL, Lao C, Wang ZL. Conversion of zinc oxide nanobelts into superlattice-structured nanohelices. *Materials Science.* 2005;309;1700–1704.
2. Cheng XL, Zhao H, Huo LH, Gao S, Zhao JG. Nanoparticute thin film, preparation, charectrarazation and gas-sensing properties. *Sensors and Actuators B.* 2004;102:248–252. http://dx.doi.org/10.1016/j.snb.2004.04.080
3. Hames Y, Alpaslan Z, Kosemen A, San SE, Yerli Y. Electrochemically grown ZnO nanorods for hybrid solar cell applications. *Solar Energy*. 2010;84:426–431.
4. Jun W, Changsheng X, Zikui B, Bailin Z, Kaijin H, Run W. Preparation of ZnO-glass varistor from tetrapod ZnO nanopowders. *Materials Science and Engineering B.* 2002;95(2):157–161. doi:10.1016/S0921-5107(02)00227-1
5. Sharma P, Sreenivas K, Rao KV. Analysis of ultraviolet photoconductivity in ZnO films prepared by unbalanced magnetron sputtering . *Journal of Applied Physics.* 2003;93:3963–3970.
6. Takumoto MS, Pulcinelli SH, Santilli CV, Briois V. Catalysis and temperature dependence on the formation of ZnO nanoparticles and of Zinc acetate derivatives prepared by the sol-gel route. *Journal of Physical Chemistry B.* 2003;107:568-574.
7. Singhal M, Chhabra V, Kang P, Shah DO. Synthesis of ZnO nanoparticles for varistor application using Zn-substituted Aerosol OT microemulsion. *Materials Research Bulletin*. 1997;32(2):239–247.
8. Rataboul F, Nayral C, Casanove MJ, Maisonnat A, Chaudret B. Synthesis and characterization of monodisperse zinc and zinc oxide nanoparticles from the organometallic precursor [Zn(C6H11)2]. *Journal of Organometalic Chemistry.* 2002;643-644:307–312.
9. Okuyama K, Lenggoro IW. Preparation of nanoparticles via spray route. *Chemical Engineering Science.* 2003;58:537–547.
10. Wei YL, Chang PC. Characteristics of nano zinc oxide synthesized under ultrasonic condition. *Journal of Physics and Chemistry of Solids.* 2008;69:688–692.
11. Arunjose L, Marylinet J, Sivasubramanian V, Akhilesh K, Justin RC, Maiyalagan, T, et al. Optical studies of nano-structured La-doped ZnO prepared by combustion method. *Materials Science in Semiconductor Processing.* 2012;15:308–313.
12. Suwanboon S, Amornpitoksuk P, Sukolrat A, Muensit N. Optical and photocatalytic properties of la-doped zno nanoparticles prepared via precipitation and mechanical milling method. *Ceramics International.* 2013;39: 2811– 2819.
13. Govindaraj R, Govindan R, Geetha M, Anbarasan PM. Structural, morphological and luminescence studies on pristine and La doped zinc oxide (ZnO) nanoparticles. *Optik International Journal for Light and Electron Optics.* 2015;126(17):1555–1558.
14. Lan W, Liu Y, Zhang M, Wang BO, Yan H, Wang Y. Structural and optical properties of La-doped ZnO films prepared by magnetron sputtering. *Materials Letters.* 2007;61(11):2262–2265. doi:10.1016/j.matlet.2006.08.061
15. Xu XL, Chen Y, Ma SY, Li WQ, Mao YZ. Excellent acetone sensor of La-doped ZnO nanofibers with unique bead-like structures. *Sensors and Actuators B: Chemical*. 2015;213: 222-233. doi:10.1016/j.snb.2015.02.073
16. Gokulakrishnan V, Parthiban S, Jeganathan K, Ramamurthi K. Investigation on the effect of Zr doping in ZnO thin films by spray pyrolysis. *Applied Surface Science*. 2011;257(21):9068–9072. doi:10.1016/j.apsusc.2011.05.102
17. Khan I, Khan S, Nongjai R, Ahmed H, Khan W. Structural and optical properties of gel-combustion synthesized Zr doped ZnO nanoparticles. *Optical Materials.* 2013;35(6):1189–1193. doi:10.1016/j.optmat.2013.01.019
18. Murtaza G, Ahmad R, Rashid MS, Hassan M, Hussnain A, Azhar Khan M, et al. Structural and magnetic studies on Zr doped ZnO diluted magnetic semiconductor.*Current Applied Physics*. 2014(2);14:176-181. doi:10.1016/j.cap.2013.11.002
19. Paul GK, Bandyopadhyay S, Sen SK, Sen S. Structural, optical and electrical studies on sol-gel deposited Zr doped ZnO films. *Materials Chemistry and Physics.* 2003;79(1):71–75. doi:10.1016/S0254-0584(02)00454-6
20. Tang MH, Zeng ZQ, Li JC, Wang ZP, Xu XL, Wang GY, et al. Resistive switching behavior of La-doped ZnO films for nonvolatile memory applications. *Solid-State Electronics*. 2011; 63(1):100–104. doi:10.1016/j.sse.2011.05.023
21. Suwanboon S, Amornpitoksuk P. Preparation and characterization of nanocrystalline La-doped ZnO powders through a mechanical milling and their optical properties. *Ceramics International.* 2011;37(8):3515–3521. doi:10.1016/j.ceramint.2011.06.007
22. Sayilkan H. Improved photocatalytic activity of Sn4+-doped and undoped TiO2 thin film coated stainless steel under UV- and VIS-irradiation. *Applied Catalysis: A.* 2007;319:230-236.
23. Moafi HF, Shojaie AF, Ali Zanjanchi M. Photoactive behavior of polyacrylonitrile fibers based on silver and zirconium co-doped titania nanocomposites: Synthesis, characterization, and comparative study of solid-phase photocatalytic self-cleaning. *Journal of Applied Polymer Science*. 2013;127(5):3778-3789. DOI: 10.1002/app.37664
24. Moafi HF, Ali Zanjanchi M, Shojaie AF. Lanthanum and Zirconium Co-Doped ZnO nanocomposites: synthesis, characterization and study of photocatalytic activity. *Journal of Nanosciencea and Nanotechnology*. 2014;14(9):7139-7150. DOI: http://dx.doi.org/10.1166/jnn.2014.8981
25. Cullity BD, Stock SR. *Elements of X-ray diffraction*. 3th ed. India: Prentice Hall; 2001.
26. Scherrer P, König A, Göttingen GW. *Mathematics Physics.* [s.l.p]: Klasse; 1918.
27. Williamson GK, Hall WH. X-ray line broadening from filed aluminium and wolfram. *Acta Metallurgica*. 1953;1(1):22–31. doi:10.1016/0001-6160(53)90006-6
28. Santra K, Chatterjee P, Sen Gupta SP. Voigt modelling of size-strain analylsis: applicaton to a-Al_2O_3 prepared by combustion technique. *Bulletin of Material Science.* 2002;25(3):251–257.
29. Prabhu YT, Venkateswara Rao K, Sesha Sai Kumar V, Siva Kumari B. X-ray analysis of Fe doped ZnO nanoparticles by Williamson-Hall and size-strain plot. *International Journal of Enginering and Advanced Technology.* 2013;2(4):268-274.
30. Moafi HF, Zanjanchi MA, Shojaie AF. Lanthanum and Zirconium Co-Doped ZnO nanocomposites: synthesis, characterization and study of photocatalytic activity. *Journal of Nanoscience and Nanotechnology*. 2014;14(9):7139-7150.
31. JCPDS. *Powder Diffraction File. Inorganic Compounds*. Newtown Square, Pa, USA: International Centre for Diffraction Data; 1977.
32. Bindu P, Sabu T. Estimation of lattice strain in ZnO nanoparticles: X-ray peak profile analysis. *Journal of Theoretical and Applied Physics*. 2014;8:123–134.
33. Pandiyarajan T, Karthikeyan B. Cr-doping induced structural, saline phonon and excitonic properties of ZnO nanoparticles. *Journal of Nanoparticle Research.* 2012;14(1):647.
34. Yogamalar, R, Srinivasan, R, Vinu, A, Ariga, K, Chandra Bose, A. X-ray peak broadening analysis in ZnO nanoparticles. *Solid State Communications*. 2009;149(43-44): 1919-1923. DOI:10.1016/j.ssc.2009.07.043.
35. Biju V, Sugathan N, Vrinda V, Salini SL. Estimation of lattice strain in nanocrystalline silver from X-ray

diffraction line broadening. *Journal of Materials Science*. 2008;43:1175–1179.

36. Nye JF. *Physical properties of Crystals: their representation by tensors and matrices*. New York: Oxford Science; 1985.
37. Yousefi R, Zak AK, Jamali-Sheini F. Growth, X-ray peak broadening studies, and optical properties of Mg-doped ZnO nanoparticles. *Materials Science in Semiconductor Processing*. 2013;16:771–777.
38. Tagliente MA, Massaro M. Strain-driven (0 0 2) preferred orientation of ZnO nanoparticles in ion-implanted silica. *Nuclear Instruments and Methods in Physics Research B:* 2008;266:1055-1061.